CrossMark

RESEARCH ARTICLE

Equilibrium Distribution of Precious Metals Between Slag and Copper Matte at 1250–1350 °C

Katri Avarmaa[1] · Hugh O'Brien[2] · Hannu Johto[1,3] · Pekka Taskinen[1]

Abstract Metal value recoveries in extraction are the key issue for sustainability of metals. The distributions of precious metals (Ag, Au, Pd, Pt, and Rh) between copper matte (a Cu–Fe–S–O melt) and silica-saturated iron silicate slag were determined at 1250–1350 °C, under controlled oxygen and sulfur pressures and at fixed partial pressure of sulfur dioxide, in silica saturation for target matte grades of 55, 65, and 75 wt% Cu. High-temperature equilibration/quenching was performed followed by electron probe X-ray microanalysis and laser ablation–inductively coupled plasma–mass spectrometry for measuring the major elements of the matte and slag, and trace elements of the slag, respectively. The distribution coefficient of silver at 65 % matte was found to be 150, which agrees well with the most recent studies in the literature. The other values obtained were gold 1500, palladium 3000, platinum 5000, and rhodium 7000–8000. The distribution coefficients increased along with matte grade, and for palladium it was approximately 1000 at 50 % Cu and 4000–5000 at 70 % Cu. The distribution coefficients decreased along with temperature but its impact was small. The distribution mechanism of the trace elements between iron silicate slag and copper matte appear to be dominated by properties of the matte phase.

✉ Pekka Taskinen
  pekka.taskinen@aalto.fi

1   Department of Materials Science and Engineering,
    Thermodynamics and Modelling Research Group, School of
    Chemical Technology, Aalto University,
    00076 Aalto (Espoo), Finland

2   Geological Survey of Finland, 02150 Espoo, Finland

3   Present Address: Boliden Harjavalta, 29800 Harjavalta,
    Finland

Introduction

The platinum group metals are typical high carbon foot-print materials of our current society [1, 2] and also among the critical metals of EU [3]. The challenges in their extraction are related to their characteristic features of being rare, occurring in the ore from which they are extracted at low concentrations (3–20 ppm total PGE), as well as in end-of-life man-made objects at trace concentrations of typically 0.1–5 ppm (g/t) [4]. Thus their material flows in various extraction and refining processes are not easily traceable until in the final stages of the entire processing chain. This allows PGEs to be easily lost in non-recoverable side streams, such as gangue, gases, and slags as well as effluents.

Precious metals are important by-products of copper and nickel smelting [5, 6]. Due to the increasing slag volume in primary copper production, metal losses in the discarded slag are becoming increasingly important in terms of recoveries and a critical issue of the resource efficiency. The recovery of precious and platinum group metals from the end-of-life products is favorably carried out in the current copper-making circuits [7] and thus this issue is emphasized also in secondary raw materials processing.

Silver is the most extensively investigated precious trace metal in the literature in terms of its behavior in sulfide smelting. Although older experimental data show disagreements regarding the level of solubility as well as the dissolution mechanism of silver in slags, recent experiments have shown that they are in good agreement with each other. Roghani et al. [8–10] did extensive research on the distribution

of silver between copper matte (0–80 % Cu) and an iron silicate slag, equilibrated in MgO crucibles. The experiments were carried out at 1250 or 1300 °C, under varying sulfur dioxide partial pressures (0.1, 0.5 and 1.0 atm). The results were nearly identical and follow the same trend: the distribution coefficient of silver $L^{m/s}$[Ag] increases linearly up to ≈ 200 at a matte grade of ≈ 65 % Cu, then drops drastically at higher Cu contents. The distribution coefficients of silver obtained in other Roghani's studies [9, 10] at a matte grade of 65 wt% Cu were between 150 and 250.

Louey et al. [11] also investigated the distribution of silver between a copper matte (50 % Cu) and an iron silicate slag. The experiments were carried out at 1250 °C under an inert N_2 gas atmosphere in MgO crucibles. The distribution coefficient of silver $L^{m/s}$[Ag] was found to be 120 ± 40. Kashima et al. [12] studied the distribution of silver in a three-phase equilibrium system of copper, white metal, and an iron silicate slag. The distribution coefficient between a Cu_2S matte (≈ 80 wt% Cu, 'white metal') and the slag was $L^{m/s}$[Ag] ≈ 20 at 1200 °C, but a considerable scatter can be found in their experimental data.

The distributions of precious metals among phases in the flash smelting process are surprisingly poorly studied. We carried out an experimental series using electron probe X-ray microanalysis techniques (EPMA) from equilibrated and quenched samples [13]. In that study, the sensitivity of EPMA for precious metals in slag restricted the reliability and success of the analyses. The most comprehensive study on distribution coefficients between copper matte and slag for Au, Pd, Pt, and Rh before that was made by Henao et al. [14]. Their experiments were done in MgO crucibles, under fixed partial pressure of sulfur dioxide (0.1 atm) for matte grades between 40 and 70 wt% Cu. It was found that the distribution coefficients $L^{m/s}$[M] were ≈ 1000 for gold, platinum, and palladium, and 100 for rhodium. A relatively large scatter was typical in the results, but the trends observed indicated that the distribution coefficients were constant in the matte grades 40–65 wt% Cu, after which they had tendency to decrease with the increasing matte grade.

The aim of the present study was the improvement of our knowledge on precious metal deportments to the iron silicate slags during smelting and converting. The previous data obtained by EPMA techniques from the equilibrated slag and matte [13] are refined in this work by a novel analytical technique allowing more accurate determination of the trace metal concentrations in the slag, with detection limits well below 1 ppm.

Experimental

The experimental techniques were based on the use of high-temperature equilibration at controlled temperature and gas atmosphere, followed by quick quenching to an ice–water mixture and direct phase analysis using EPMA and laser ablation–inductively coupled plasma–mass spectrometry (LA-ICP-MS). Although the equilibration technique applied has been used widely for slag or even slag/matte studies [14–16], this was the first time when it was adopted to study the distributions of trace elements. The LA-ICP-MS technique adopted for the slags has much lower detection limits than the EPMA used earlier [13]. Moreover, this is the second study to investigate the effect of temperature on the distribution coefficients of precious metals [13].

The main features of the experimental setup were a vertical high temperature tube furnace (Lenton PTF 15/-/450) using Eurotherm PID controllers, the gas inlet system using mass flow controllers (Aalborg 052-01-SA), and accurate temperature measurement (a calibrated S-type thermocouple) with Keithley data logging. Details of the experimental setup are available elsewhere [13]. Copper matte and iron silicate slag were equilibrated at 1250, 1300, or 1350 °C under controlled CO–CO_2–SO_2–Ar gas atmospheres, in pure silica crucibles. CO–CO_2–SO_2–Ar gas mixtures were used to generate specific partial pressures of SO_2, O_2, and S_2 in the furnace at the experimental temperature. The partial pressure of SO_2 was held constant (0.09 $\pm$ 0.015 atm), and the partial pressures of O_2 and S_2 were fixed to a certain target matte grade (55, 65, or 75 wt% Cu), in each experiment, see Table 1. Argon was added to the gas mixture in order to increase the flow rate. Nitrogen gas was used as purge gas after the experiments. The oxygen and sulfur partial pressures were defined from Yazawa diagram [17] for certain matte grades at $p(SO_2) = 0.1$ atm and 1300 °C. Then the temperature dependence and $CO/CO_2/SO_2$ ratios were scaled and calculated using the MTDATA software [18] and SGTE pure substance database [19] to correspond with the defined partial pressures of Yazawa diagram. As the target matte grade was known, it was possible to verify the success of the calculations from the obtained results.

The matte analyses were done with EPMA using a Cameca SX100 equipped with five Wavelength Dispersive spectrometers (WDS). The matte had its own special features [13]—in spite of using a quick quenching process, the precious metals nevertheless segregated as very fine exsolution blebs and lamellae. Attention was paid to this feature when attempting to get analyses of the true bulk equilibrium matte composition. To reintegrate the PGE exsolution features, a broad 100 µm electron beam spot was used and 10 analyses per matte were averaged, giving reliable bulk analyses with an estimated instrumental uncertainty of analyses of $<\pm 0.5$ wt%. Cameca uses the PAP correction [20] for the matrix effects [21] to perform accurate quantitative analyses (Table 2).

Laser ablation single collector ICP-MS analyses of experimental slags were performed using an Nu AttoM SC-

ICPMS (Nu Instruments Ltd., Wrexham, UK) and an Analyte G2 193 nm ArF laser ablation system (Teledyne CETAC Technologies, Omaha, USA). The laser was run at a pulse frequency of 10 Hz and a pulse energy of 4 mJ at 48 % attenuation to produce a energy flux of 2.65 J/cm^2 on the sample surface with a 50-µm spot size. The laser was automatically switched on for 60 s for signal acquisition and then off for 20 s for background levels to be attained and measured. Analyses were made using time-resolved analysis (TRA) with continuous acquisition of data for each set of points (2 standards, 10 unknown glasses, 1 quality control standard). The USGS reference glass BHVO-2G was used for quality control although PGE contents are relatively inhomogeneous in this glass [22]. Synthetic NIST SRM 612 glass (concentrations reported in Jochum et al. [23]) and ^{29}Si have been used, respectively, as external and internal standards for quantification. The measurements were performed over 26 elements (Li, Si, Fe, Sr, Rh, Pd, Ag, La, Ce, Pr, Nd, Sm, Eu, Gd, Tb, Dy, Ho, Er, Tm, Yb, Lu, Pt, Au, Pb, Th, U) at low resolution ($\Delta M/M = 300$) using the fast scanning mode. Baseline reduction of the trace element data was performed using Iolite v. 2.5 software [24] run within the Igor Pro 6.32A host environment. Quantification was then proceeded by Excel spreadsheet data handling using known concentrations in the NIST SRM 612, the measured Si^{29} signal, which corrects for the differences in laser absorption of glasses of varying color, and the SiO$_2$ concentration of each individual glass, measured previously by the electron microprobe. The instrumental uncertainty of the LA-ICP-MS technique was ±5–10 wt%. The slag analyses were done from well-quenched areas avoiding the segregations of matte droplets; nevertheless, slag inhomogenities contributed to elemental standard deviations in excess of 20 % in some samples.

Two series of experimental runs were carried out in order to determine distribution coefficients for the precious metals Rh, Ag, Pt, Au, and Pd between the slag and copper matte in silica-saturated conditions. The specimens for microanalysis were prepared by breaking the crucibles and mounting the samples in epoxy resin. The polished sections were prepared using traditional wet metallographic methods (grinding, polishing, and an optical microscope). The polished surfaces were carbon coated. Their microstructures and phase compositions were pre-examined using SEM–EDS techniques before the EPMA and LA-ICP-MS measurements.

Results

The primary analytical results from the experiments are listed in Tables 2 and 3. Each experimental point in the tables is an average value of 10 independent measurements for the slag and matte, respectively. The matte grade in most of the experiments was approximately 5 wt% lower than that expected. In our previous paper [13], we suggested this was caused by the added precious metals which replaced other metals (Fe, Cu) in the structure of the molten matte.

Oxygen was analyzed in the first series only and the values for the second series were estimated based on iron concentrations. The matte grades in the following figures are normalized analytical data calculated from the primary results.

Trace Metal Concentrations in the Silica-Saturated Iron Silicate Slag

The precious metal concentrations dissolved in silica-saturated iron silicate slags in equilibrium with sulfidic copper mattes were typically between 5 and 20 ppm. Silver is an exception, exhibiting significantly higher solubility than the other trace elements studied, but in all experiments

Table 1 Gas atmospheres (flow rates, STP) and temperatures in the experimental points studied

Experimental temperature °C	Target matte grade (wt-% Cu)	Target Log P_{O_2} atm	Target Log P_{S_2} (atm)	CO flow rate (mL/min)	CO$_2$ flow rate (mL/min)	SO$_2$ flow rate (mL/min)	Ar flow rate (mL/min)	Equilibration test: code
1250	55	−8.4	−2.3	10	50	35	300	Ka33, Ka50
1250	65	−8.2	−2.7	7	50	35	300	Ka34, Ka51
1250	75	−7.9	−3.4	4	50	35	300	Ka41, Ka53
1300	55	−8.1	−2.2	12	15	40	300	Ka36, Ka46
1300	65	−7.9	−2.6	12	55	40	300	Ka31, Ka47
1300	75	−7.6	−3.3	6	55	40	300	Ka32, Ka48
1350	55	−7.8	−2.1	12	5	40	300	Ka38, Ka43
1350	65	−7.6	−2.5	12	34	45	300	Ka39, Ka44
1350	75	−7.3	−3.2	8	55	45	300	Ka40, Ka45

Table 2 EPMA results for copper mattes studied at various temperatures

Target matte grade [%Cu]	Experiment label	Matte analysis ± standard deviation (wt%)									
		Fe	Cu	S	Rh	Ag	Pt	Au	Pd	O	Total
1250 °C, 55	Ka33	14.43 ± 0.12	56.71 ± 0.36	23.44 ± 0.12	1.04 ± 0.06	0.97 ± 0.06	1.19 ± 0.10	0.65 ± 0.08	1.10 ± 0.09	1.86 ± 0.14	101.42
	Ka50	13.13 ± 0.17	57.23 ± 0.43	22.46 ± 0.13	1.00 ± 0.06	0.93 ± 0.07	1.04 ± 0.10	0.98 ± 0.12	1.01 ± 0.07	n.a.	
1250 °C, 65	Ka34	8.63 ± 0.16	64.66 ± 0.47	22.16 ± 0.17	0.87 ± 0.06	1.03 ± 0.07	0.81 ± 0.14	0.85 ± 0.15	1.02 ± 0.09	1.46 ± 0.13	101.49
	Ka51	8.46 ± 0.17	64.27 ± 0.48	21.47 ± 0.15	0.73 ± 0.14	1.06 ± 0.13	0.43 ± 0.16	0.80 ± 0.16	1.15 ± 0.13	n.a.	
1250 °C, 75	Ka41	3.63 ± 0.07	71.03 ± 0.60	19.97 ± 0.20	0.89 ± 0.04	0.97 ± 0.42	0.64 ± 0.08	0.47 ± 0.10	1.38 ± 0.10	1.16 ± 0.10	100.14
	Ka53	3.33 ± 0.01	70.25 ± 0.76	19.96 ± 0.17	0.97 ± 0.08	1.11 ± 0.12	0.60 ± 0.05	1.10 ± 0.10	1.19 ± 0.10	n.a.	
1300 °C, 55	Ka36	20.18 ± 0.51	50.03 ± 0.95	24.38 ± 0.28	0.83 ± 0.08	0.84 ± 0.05	0.74 ± 0.13	0.50 ± 0.12	0.97 ± 0.07	2.61 ± 0.24	101.09
	Ka46	21.24 ± 0.24	48.97 ± 0.50	24.09 ± 0.21	0.81 ± 0.05	0.77 ± 0.06	0.71 ± 0.08	0.68 ± 0.10	0.98 ± 0.07	n.a.	
1300 °C, 65	Ka31	12.43 ± 0.09	59.07 ± 0.36	22.71 ± 0.11	1.00 ± 0.09	0.74 ± 0.12	1.00 ± 0.06	0.84 ± 0.08	1.23 ± 0.08	1.77 ± 0.11	100.79
	Ka47	11.46 ± 0.18	60.37 ± 0.57	22.29 ± 0.12	0.95 ± 0.10	0.88 ± 0.08	1.19 ± 0.08	0.57 ± 0.04	1.08 ± 0.09	n.a.	
1300 °C, 75	Ka32	3.50 ± 0.06	71.03 ± 0.40	20.43 ± 0.12	1.02 ± 0.11	0.84 ± 0.12	0.80 ± 0.11	0.75 ± 0.12	1.38 ± 0.08	1.38 ± 0.22	101.14
	Ka48	3.56 ± 0.09	70.25 ± 0.55	20.34 ± 0.13	0.93 ± 0.34	1.03 ± 0.13	0.80 ± 0.34	0.55 ± 0.07	1.27 ± 0.13	n.a.	
1350 °C, 55	Ka38	20.02 ± 0.22	49.66 ± 1.11	23.95 ± 0.23	0.83 ± 0.11	0.47 ± 0.05	1.36 ± 0.21	0.53 ± 0.09	0.92 ± 0.12	2.53 ± 0.20	100.31
	Ka43	19.53 ± 0.50	50.99 ± 0.94	23.65 ± 0.26	0.82 ± 0.08	0.61 ± 0.05	0.93 ± 0.14	0.79 ± 0.15	0.94 ± 0.08	n.a.	
1350 °C, 65	Ka39	11.92 ± 0.17	60.37 ± 0.71	22.50 ± 0.15	0.94 ± 0.12	0.47 ± 0.12	0.91 ± 0.22	0.99 ± 0.12	1.21 ± 0.14	1.79 ± 0.16	101.11
	Ka44	11.35 ± 0.23	60.68 ± 0.60	21.99 ± 0.12	1.04 ± 0.06	0.58 ± 0.06	1.18 ± 0.12	1.38 ± 0.18	1.11 ± 0.13	n.a.	
1350 °C, 75	Ka40	4.21 ± 0.12	69.51 ± 0.44	20.68 ± 0.12	0.83 ± 0.19	0.55 ± 0.04	0.83 ± 0.32	0.77 ± 0.13	1.27 ± 0.17	1.21 ± 0.11	99.87
	Ka45	3.84 ± 0.10	71.11 ± 0.55	20.61 ± 0.11	0.84 ± 0.15	0.53 ± 0.10	1.01 ± 0.22	0.60 ± 0.15	1.08 ± 0.11	n.a.	

Data represent averages and standard deviations on 10 analytical points per sample

Table 3 LA-ICP-MS results for iron silicate slags at various temperatures and copper grades

Target: T/°C, [%Cu]	Experiment label	Average ±standard deviation (ppm)				
		Rh	Pd	Ag	Pt	Au
1250, 55	Ka33	1.78 ± 0.33	5.72 ± 0.62	70.8 ± 11.1	4.91 ± 0.92	8.85 ± 1.41
	Ka50	1.31 ± 0.31	5.43 ± 1.06	77.3 ± 15.2	3.58 ± 0.79	19.19 ± 5.29
1250, 65	Ka34	1.03 ± 0.23	3.29 ± 0.64	66.1 ± 8.2	1.59 ± 0.30	6.96 ± 1.07
	Ka51	0.89 ± 0.13	3.62 ± 0.44	64.0 ± 6.3	1.20 ± 0.14	5.58 ± 0.64
1250, 75	Ka41	0.73 ± 0.04	2.41 ± 0.19	54.2 ± 14.4	0.42 ± 0.05	1.24 ± 0.12
	Ka53	0.75 ± 0.04	2.60 ± 0.36	65.1 ± 7.7	0.51 ± 0.05	3.15 ± 0.16
1300, 55	Ka36	1.50 ± 0.28	4.50 ± 1.30	41.3 ± 11.2	3.90 ± 0.90	9.30 ± 2.00
	Ka46	2.63 ± 0.69	9.26 ± 2.61	68.9 ± 23.3	6.31 ± 1.67	20.80 ± 6.21
1300, 65	Ka31	1.61 ± 0.18	6.09 ± 0.76	56.4 ± 9.7	3.47 ± 0.48	11.42 ± 1.79
	Ka47	1.30 ± 0.28	4.24 ± 1.01	53.7 ± 12.1	3.34 ± 0.73	5.59 ± 1.22
1300, 75	Ka32	1.25 ± 0.23	4.02 ± 0.83	51.5 ± 12.3	3.17 ± 0.61	5.34 ± 1.18
	Ka48	0.98 ± 0.14	3.17 ± 0.48	74.5 ± 13.3	0.66 ± 0.08	2.03 ± 0.25
1350, 55	Ka38	3.26 ± 0.60	10.30 ± 1.83	39.9 ± 11.5	14.62 ± 3.95	12.17 ± 3.10
	Ka43	2.30 ± 0.50	8.37 ± 2.07	59.3 ± 13.8	7.34 ± 1.58	20.43 ± 4.6
1350, 65	Ka39	1.77 ± 0.17	5.58 ± 0.51	46.1 ± 11.7	3.50 ± 0.34	13.52 ± 1.19
	Ka44	1.79 ± 0.25	6.07 ± 0.83	51.9 ± 12.0	4.55 ± 0.65	17.24 ± 3.18
1350, 75	Ka40	1.08 ± 0.19	3.50 ± 0.73	37.7 ± 8.7	0.91 ± 0.12	2.84 ± 0.40
	Ka45	1.10 ± 0.07	3.47 ± 0.39	41.5 ± 6.0	1.00 ± 0.04	2.37 ± 0.30

Data represent averages and standard deviations on 10 analytical points per sample

remaining below 100 ppm. Results for Ag as a function of the matte grade are shown in Fig. 1. The uncertainties given in the graphs are standard deviations (±1σ) of the measurements by LA-ICP-MS. The temperature dependencies of the precious metals concentrations were in general small, except in the case of silver. The solubilities decrease as a function of increasing Cu% in the matte in all cases.

As the trend lines at 1250 and 1350 °C indicate, the temperature dependence of silver solubility in silica-saturated iron silicate slags from copper matte is large. One factor influencing this feature may be the observed high volatility of silver, decreasing systematically the silver concentration of the studied mattes at high temperatures [13]. For example, through volatilization, experiments Ka38 and Ka39 lost over half of their initial silver, dropping from an initial ≈1 % [Ag]$_{matte}$ to final compositions with only ≈0.47 % [Ag]$_{matte}$. However, the amount of silver deported in the slag is negligible compared to the silver concentration in the matte in all experiments.

The concentrations of gold, palladium, platinum, and rhodium in the slag as measured by the LA-ICP-MS technique are shown in Figs. 2, 3, 4, and 5. The scatter of the observed concentrations between the experiments in same conditions is about ±20 % of the measured concentration. The Ka36 sample at 50 % matte grade and 1300 °C shows systematically lower solubilities for all trace
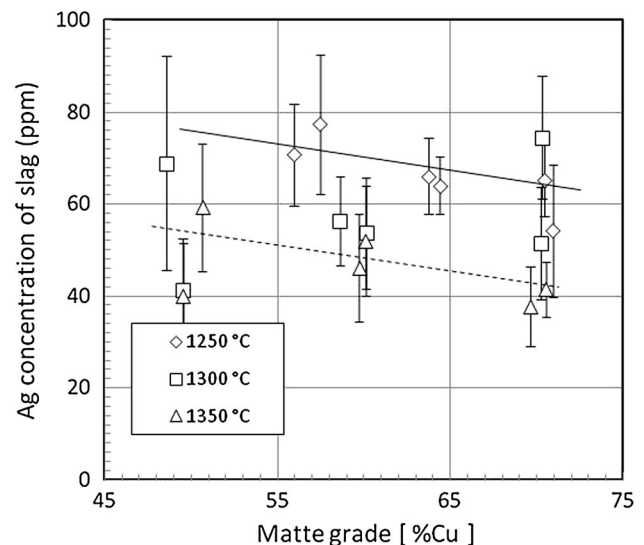

Fig. 1 The measured silver concentrations in the silica-saturated iron silicate slag at 1250–1350 °C as a function of the matte grade, i.e., wt% Cu in matte; the initial silver concentration prior to the equilibration was ≈1 % [Ag]$_{matte}$; the trend lines (*solid line* at 1250 °C and *dotted line* at 1350 °C) were calculated for two temperatures only; the *error bars* give standard deviations of the measurements (±1σ)

elements, except for silver. Laser Ablation time-resolved analysis profiles for this sample were exceptionally noisy reflecting heterogeneities and potential matte inclusions.

As Figs. 1, 2, 3, 4, and 5 indicate vividly, the solubility of the studied precious metals in the silica-saturated slag in slag–matte equilibrium decreased systematically when the matte was enriched by copper. The only exception in the present study is silver where concentration versus matte trade plot shows no clear trend due to the large deviations in Ag contents measured from each sample. In general, the standard deviations of Ag concentrations in the slags are at least two times higher than the deviations for other precious metals. This is despite the higher concentration of Ag, and hence more precise measurements of Ag concentrations. This observation may indicate a difference in the matte–slag distribution behavior of Ag relative to the PGEs and Au.

Figures 2, 3, 4, and 5 indicate that the solubilities of the studied platinum group elements (PGEs) in the slags are clearly lower than that of gold over the entire compositional range of matte studied in this work. Gold distributing from high-iron mattes with about 50 % Cu is about an order of magnitude higher than from white metal compositions, close to blister copper saturation (Fig. 2). The same trend is visible in the studied PGEs, as shown in Figs. 3, 4, and 5, but the effect is not as large as in the case of gold.

Distribution Coefficients

The trace element distribution coefficients are linked with their thermodynamic properties in the matte and slag phases. They were calculated from the measured concentrations based on the definition:

$$L^{m/s}[\text{Me}] \equiv [\text{ppm Me}]/(\text{ppm Me}), \qquad (1)$$

where the brackets [] and () refer to the matte and slag phases in equilibrium, respectively. The trace element distribution coefficients were calculated from the primary measurement data separately at each experimental point of the slag-to-matte equilibrium. The results with a different symbol for each temperature are shown in Figs. 6, 7, 8, 9, and 10 with matte grade as the x-axis variable.
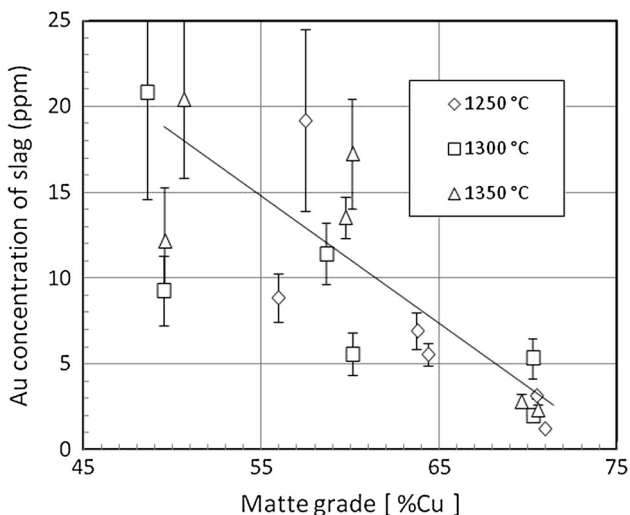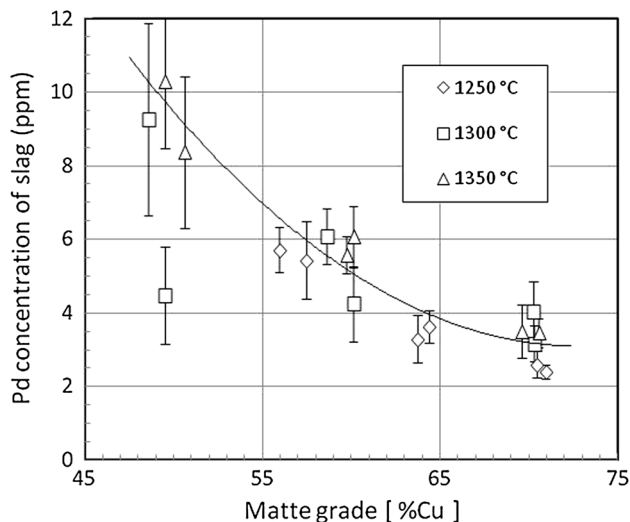

Fig. 3 Palladium concentrations in the silica-saturated iron silicate slag at 1250–1350 °C as a function of the matte grade; the initial palladium concentration prior to the equilibration was ≈ 1 % $[\text{Pd}]_{\text{matte}}$; the trend line (*soild line*) has been drawn based on the experimental points, omitting sample Ka36

Fig. 2 Gold concentrations in the silica-saturated iron silicate slag at 1250–1350 °C as a function of the matte grade; the initial gold concentration prior to the equilibration was ≈ 1 % $[\text{Au}]_{\text{matte}}$; the trend line (*solid line*) has been drawn based on the experimental points, omitting sample Ka36
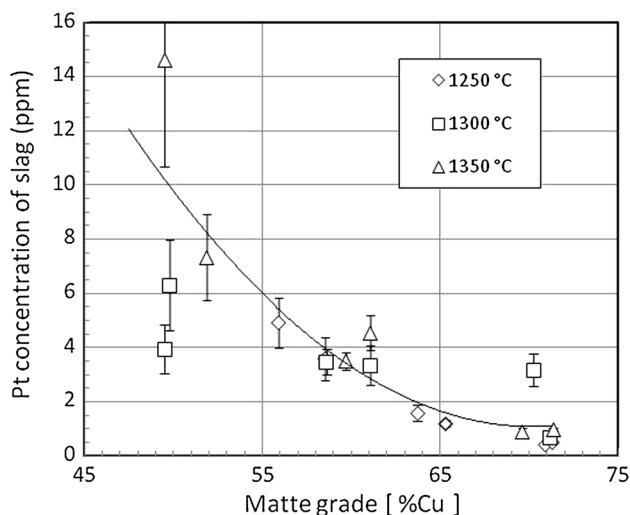

Fig. 4 Platinum concentrations in the silica-saturated iron silicate slag at 1250–1350 °C as a function of the sulfide matte grade; the initial platinum concentration prior to the equilibration was ≈ 1 % $[\text{Pt}]_{\text{matte}}$; the trend line (*solid line*) has been drawn based on the experimental points, omitting sample Ka36
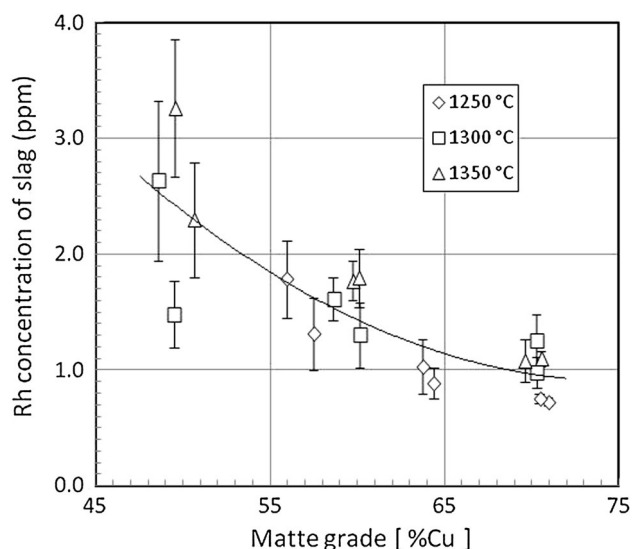
Fig. 5 The observed rhodium concentrations in the silica-saturated iron silicate slag at 1250–1350 °C as a function of the matte grade; the initial rhodium concentration prior to the equilibration was ≈1 % [Rh]$_{matte}$; the trend line (*solid line*) has been drawn based on the experimental points, omitting sample Ka36
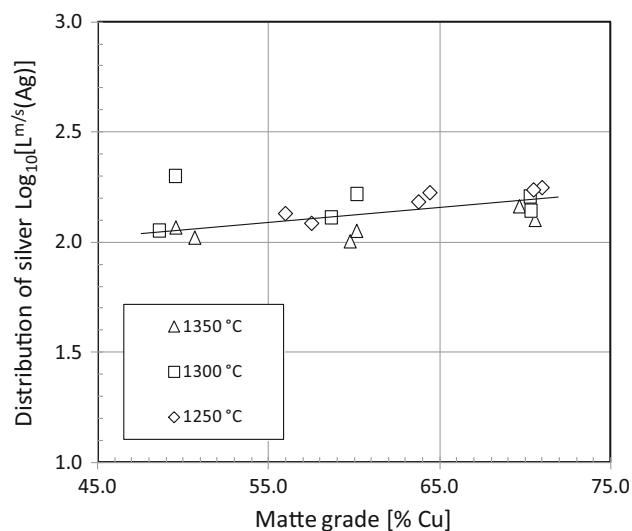

Fig. 7 Logarithmic distribution coefficient of gold between silica-saturated iron silicate slag and copper matte at 1250–1350 °C and in P(SO$_2$) = 0.1 atm as a function of the analyzed matte grade of the sulfide matte; *trendline* shows the behavior of the 1350 °C data

Fig. 6 Logarithmic distribution coefficient of silver between silica-saturated iron silicate slag and copper matte at 1250–1350 °C and in P(SO$_2$) = 0.1 atm as a function of the analyzed matte grade of the sulfide matte; the trend line (*solid line*) has been drawn based on the experimental points, omitting sample Ka36

Fig. 8 Logarithmic distribution coefficient of palladium between silica-saturated iron silicate slag and copper matte at 1250–1350 °C and in P(SO$_2$) = 0.1 atm as a function of the analyzed matte grade of the sulfide matte; *trendline* shows the behavior of the 1350 °C data

Figure 6 shows the distribution coefficient of silver L[Ag] according to the definition of Eq. (1) as a function of the matte grade at 1250, 1300, and 1350 °C. The trendline shown in the figure is based on the experimental points at 1350–1250 °C. The distribution of silver favors the matte phase when the oxygen pressure of the sulfide matte–slag–gas system gets higher and thus the matte grade increases. The distribution coefficient is roughly doubled when the
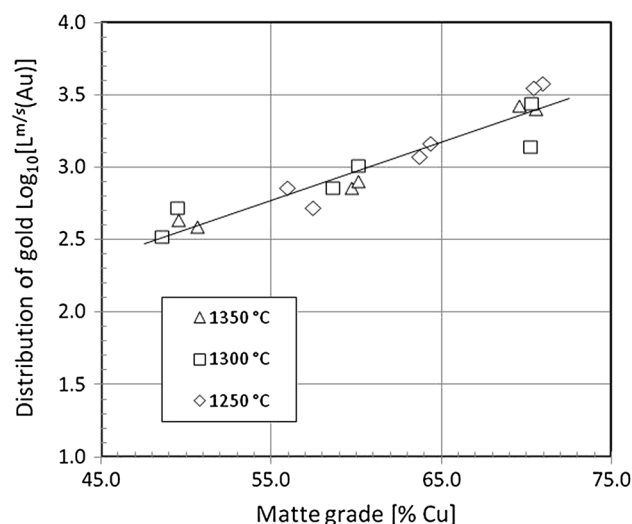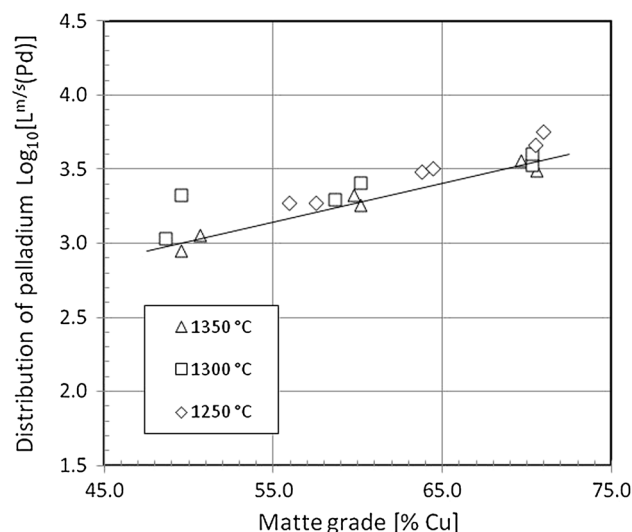
matte grade grows from ≈50–70 % Cu. Although the temperature dependence is small, the results indicate that the deportment of silver to the sulfide matte is favored by low-temperature processes.

The corresponding distribution coefficients for gold, palladium, platinum and rhodium calculated from the measured average concentrations in the matte and slag are depicted in Figs. 7, 8, 9, and 10, respectively. They all show a clear increasing trend as a function of the matte grade. Although temperature dependencies of the distribution
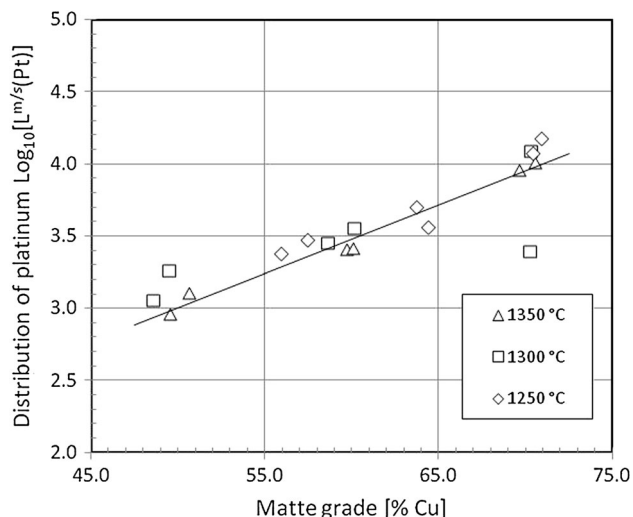
Fig. 9 Logarithmic distribution coefficient of platinum between silica-saturated iron silicate slag and copper matte at 1250–1350 °C and in P(SO$_2$) = 0.1 atm as a function of the analyzed matte grade of the sulfide matte; *trendline* shows the behavior of the 1350 °C data
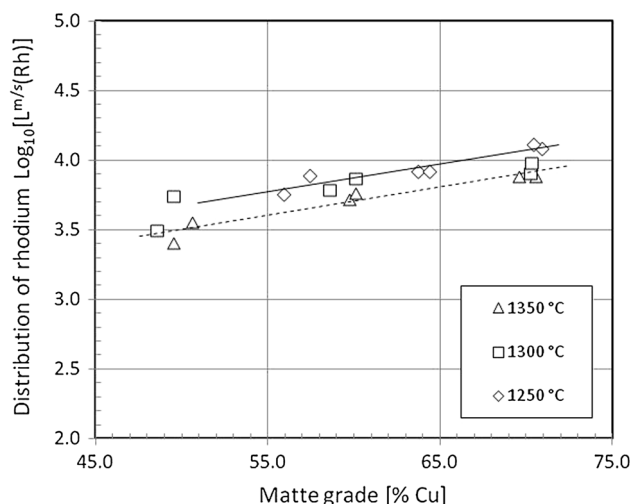

Fig. 10 Logarithmic distribution coefficient of rhodium between silica-saturated iron silicate slag and copper matte at 1250–1350 °C and in P(SO$_2$) = 0.1 atm as a function of the analyzed matte grade of the sulfide matte; the *trend lines* have been calculated at 1250 °C (*solid line*) and 1350 °C (*dotted line*)

coefficients are generally relatively small, as a general trend, low temperature favors partitioning of the trace elements into the matte phase.

In Fig. 10, the trend lines have been drawn for the experimental points obtained at 1250 and 1350 °C, indicating the effect of process temperature on the distribution coefficient $L^{m/s}$ of rhodium. In the other cases, the temperature dependence obtained was too small to indicate any significant impact of the process temperature.

Discussion

The results of this study show that the solubility of precious metals in slag is almost negligible. Thus, it can be deducted that in the flash smelting copper-making process, the losses of precious metals are dominated by matte entrainment, i.e. mechanical losses rather than chemical dissolution.

The trace element solubility values in the slag from dilute solutions in copper mattes obtained in this work, Figs. 1, 2, 3, 4, and 5, indicate that the growing distribution coefficients between matte and slag result from deportment of the trace elements in the matte by depletion of the slag. The experimental range of this study covered the entire range of matte flash smelting conditions from very lean copper mattes of 50 % Cu to rich mattes with 70 % Cu, at typical temperature from 1250 to 1350 °C. As the oxidic solubility of the elements increases along with the growing oxygen partial pressure of the system [25, 26] when the copper sulfide matte is enriched in copper, the increase in $L^{m/s}$ is evidently not due to the properties of the slag, but rather conditions in the sulfide matte wherein iron and sulfur concentrations as well as sulfur-to-metal ratios are decreasing.

The observed concentrations of the precious metals in the silica-saturated iron silicate slags in our experiments are lower than those reported by previous authors [13, 14]. The distribution coefficients between copper matte and the silica-saturated slag increased systematically as a function of the matte grade in our study. Thus, no decrease in $L^{m/s}$ [Me] was seen at high matte grades close to the white metal compositions, or iron-free copper sulfide [8], prior to copper saturation. The highest matte grade in the present study was $\approx$ 72 % Cu and our results indicate systematic increase in L$^{m/s}$[Me] as the matte was depleted in iron and its oxygen partial pressure increased. This confirms the qualitative trends reported earlier [13].

The behavior of the distribution coefficients derived in this study cannot be explained by conventional oxidation–sulfidation equilibria [13] as the present observations clearly indicate that the slag is depleted in trace elements with the increasing matte grade. This is evidently a result of the properties of copper matte when its sulfur-to-metal stoichiometry changes. Its behavior is characterized by the gradual oxidation of sulfur from the matte as the iron concentration decreases [27, 28]. Lynch et al. [27] introduced the concept of sulfur deficiency SD and the number of 'vacant electronegative sites in the (oxygen-free) matte' as

$$SD \equiv x_S - x_{Cu}/2 - x_{Fe}, \qquad (2)$$

where x_i are the molar fractions of sulfur, copper and iron, respectively. It is approximately zero on the Cu$_2$S–FeS quasibinary join of the Cu–Fe–S system, negative for matte

compositions on the metal-rich side of the join and positive on the sulfur-rich side. It was proposed by Lynch et al. [27] that the excess metal species in sulfur-depleted mattes interact with copper and iron of the matte which thus modifies their properties. Thus the thermodynamic features of trace elements in matte–copper equilibrium may be very different from those in the copper mattes elsewhere within its stability range [29, 30], typically along the quasibinary Cu_2S–FeS join or in sulfur-rich mattes. Therefore, we modified the equation of sulfur deficiency for the current equilibrium case and used the variable SD″ as

$$SD'' \equiv x_S + x_O - x_{Cu}/2 - x_{Fe} - \Sigma x_{Me}, \qquad (3)$$

where x_S, x_O, and x_{Me} are the molar fractions of sulfur, oxygen, and the trace elements of the matte phase, respectively. This variable was used for the correlations of the present data in order to indicate qualitatively the trends in the (logarithm) of the activity coefficient of the trace elements in the matte, see Figs. 11, 12, 13, 14, and 15. As shown in the figures, the studied mattes have a slight excess of sulfur as their estimated sulfur deficiencies were positive, around $SD'' = 0.02–0.06$. The values were calculated from the normalized data of Table 2.

In case of silver, the distribution results of this investigation and the recent studies in the literature [8–10, 13] agree well with each other but techniques with slow cooling result in much higher distribution coefficients [31]. Some earlier authors [12, 32, 33] suggested that silver exists in iron silicate slags as metallic species. According to Richardson and Billington [32], neutral silver atoms in a molten silicate slag are located in holes of the silicate
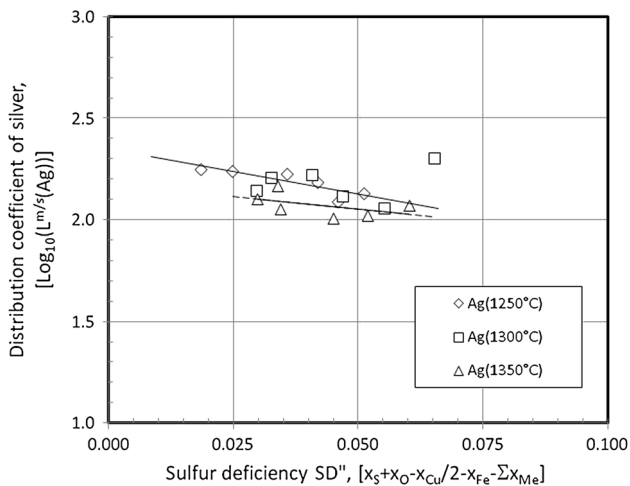
network. It was also proposed [9, 34] that at low matte grades, silver exists in the slag as silver sulfide species, typically $AgS_{0.5}$. When matte grade increases, sulfur activity and SD decrease, sulphidic silver solubility to matte gradually decreases. In studies between metallic copper and iron silicate as well as calcium ferrite slags, the dependency between distribution coefficient and oxygen partial pressure indicated [10, 35] that silver dissolves to the slag as monovalent silver oxide species (as Ag_2O or $AgO_{0.5}$) in the partial pressures $P_{O2} = 10^{-11}–10^{-5}$ atm. The limiting silver–copper system is essentially an ideal
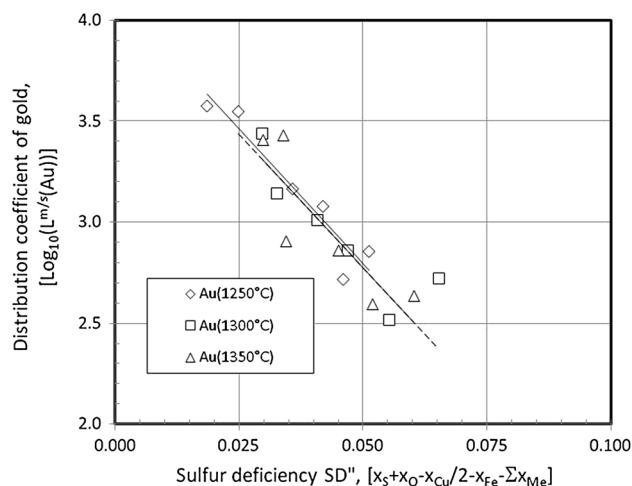

Fig. 12 The behavior of the matte-to-slag logarithmic distribution coefficient of gold as a function of the sulfur deficiency of the copper matte at 1250–1350 °C; the linear trend lines show the slopes of the experimental points calculated at 1250 (*solid line*) and 1350 °C (*dotted line*)

Fig. 11 The behavior of the matte-to-slag logarithmic distribution coefficient of silver as a function of the sulfur deficiency of the copper matte at 1250–1350 °C; the linear trend lines calculated at 1250 (*solid line*) and 1350 °C (*dotted line*) show the slopes of the experimental points
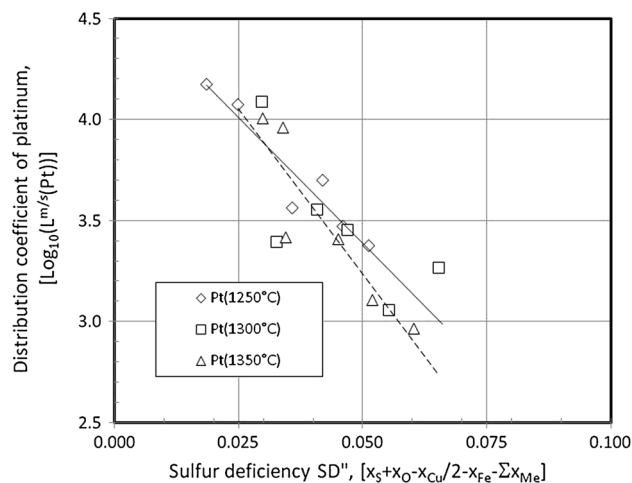

Fig. 13 The behavior of the matte-to-slag logarithmic distribution coefficient of platinum as a function of the sulfur deficiency of the copper matte at 1250–1350 °C; the linear trend lines show the slopes of the experimental points calculated at 1250 (*solid line*) and 1350 °C (*dotted line*)
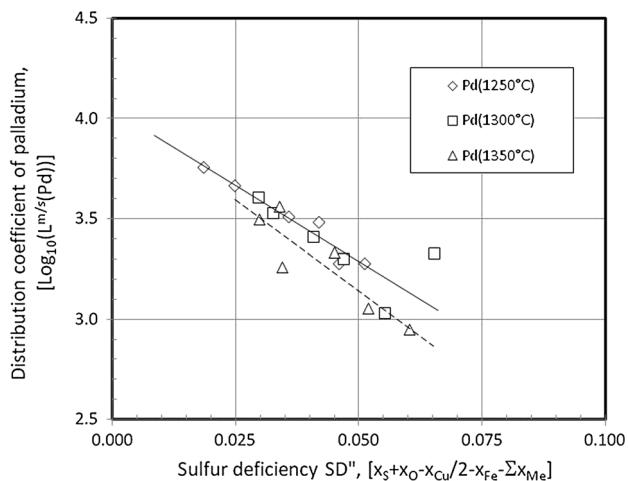
Fig. 14 The behavior of the matte-to-slag logarithmic distribution coefficient of palladium as a function of the sulfur deficiency of the copper matte at 1250–1350 °C; the trend lines calculated at 1250 (*solid line*) and 1350 °C (*dotted line*) show the slopes of the experimental points
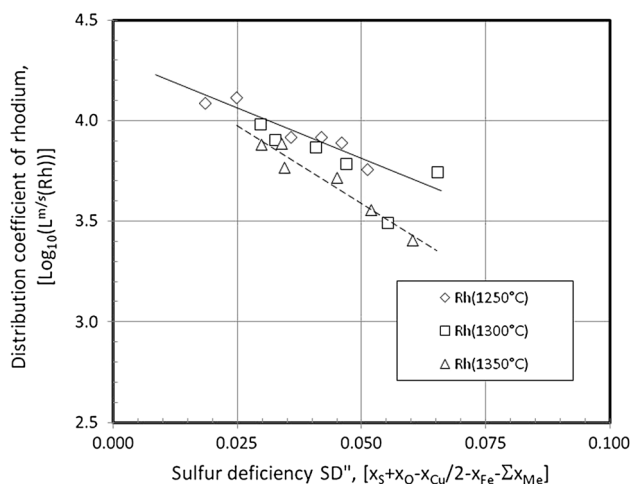

Fig. 15 The behavior of the matte-to-slag logarithmic distribution coefficient of rhodium as a function of the sulfur deficiency of the copper matte at 1250–1350 °C; the linear trend lines show the slopes of the experimental points calculated at 1250 (*solid line*) and 1350 °C (*dotted line*)

solution [36] but the activity coefficient of silver is about 10 in copper sulfide [37]. This experimental finding indicates the role of matte and its stoichiometry to the thermodynamics of trace element it contains.

According to the present study, the distribution coefficient clearly increases and the solubility of gold decreases as the matte grade is enriched at all temperatures studied. The distribution coefficient of gold in this study, ≈ 400 at 50 % and 3000 at 70 % matte grade, was close to the results obtained by previous authors [8, 13, 38]. In some studies, the distribution coefficient decreased as a function

of the matte grade [14], and in the others gold solubility in the slag increased as a function of the growing oxygen partial pressure [13, 38]. However, the distribution coefficient between Ni and Cu matte and iron silicate slag showed an increasing trend along with the growing matte grade [38–40]. Copper–gold system shows a negative deviation from ideal behavior for gold in dilute copper alloys [36].

The distribution coefficients obtained for platinum were larger than those reported by Henao et al. [14] and in our previous paper [13]. According to Yamaguchi [41], the solubility of pure platinum in a FeO_x–SiO_2 slag (i.e., slag in equilibrium with pure platinum) was 3–7 ppm at $P_{O2} = 10^{-8}$–10^{-6} atm, and it was 100–1000 ppb at $P_{O2} = 10^{-8}$–10^{-7} atm in silicate melts of basaltic composition [42–44]. These data fit well with the results of this study. In the previous studies, the $L^{m/s}[Pt]$ distribution coefficient decreased along with the increasing matte grade [14] and the distribution coefficient between metal and slag, $L^{Cu/s}[Pt]$, decreased with the increasing P_{O2} [45]. Such features were not detected in this study. However, according to Mungall and Brennan [25], the solubility of platinum in basaltic melts depends on the oxygen partial pressure, e.g., in the P_{O2} range of $10^{-8.5}$–$10^{-5.5}$ atm, the solubility systematically increased from 9 to 97 ppb as a function of temperature at 1200–1500 °C. The iron matte–basalt distribution data at 1200 °C and QFM-1 gave $L^{m/s}[Pt] > 10^5$ which is much higher than the present value. There is also evidence that Pt solubility increases in the presence of sulfur [19]. Platinum in dilute solutions of copper shows negative deviation from Raoult's law [46].

The trend of palladium distribution obtained, an increasing distribution coefficient with the increasing matte grade, is in conflict with the previous studies of copper smelting and geological low-iron (silicate) systems, except [13]. In those studies, the distribution coefficients $L^{m/s}[Pd]$ and $L^{Cu/s}[Pd]$ decreased along with the increasing matte grade and oxygen partial pressure [8, 45], respectively, and palladium content of the slag increased [42–45]. The solubility of palladium in basaltic melts (i.e., sulfur free in equilibrium with pure palladium) at 1200–1500 °C was found to be 1.6–13 ppm at $P_{O2} = 10^{-8.5}$–$10^{-5.5}$ atm (close to the QFM equilibrium buffer, i.e., the solid quartz–fayalite–magnetite equilibrium) [42–44], which fits well with the observations of this study. Recent LA-ICP-MS data by Mungall and Brenan [25] at QFM-1 (i.e., at oxygen pressure of $Log_{10} P_{O2} = -9.40$) at 1200 °C produced an iron matte–basalt distribution coefficient $L^{m/s}[Pd] > 10^5$. Palladium–copper alloys deviate negatively from Raoultian behavior in the dilute palladium systems [47].

The solubility of rhodium in the silica-saturated silicate slag was the lowest among the PGEs studied in this work, showing a minimum concentration of around 0.7–0.8 ppm

(Rh) at 70 % matte grade. In the study of Henao et al. [14], the matte-to-slag distribution coefficients of rhodium were approximately 100. In the geological literature for hap-lobasaltic melt (the anorthite–diopside eutectic), the solubility of rhodium (i.e., in equilibrium with pure rhodium) at 1300 °C was only 10–100 ppb at $P_{O2} = 10^{-9}$–10^{-6} atm[48–50]. Iron matte–slag–basalt distribution data [25] at 1200 °C and QFM-1 provided a rhodium distribution coefficient $L^{m/s}[Rh] > 10^5$ which is about one order of magnitude higher than the values presented here. The thermodynamic properties of rhodium in dilute liquid copper–rhodium alloys show positive deviation from the Raoultian behavior [36].

The current results indicate that the precious metals are increasingly distributed into the copper matte relative to the silica-saturated iron silicate slag when the prevailing oxygen pressure during the process systematically increases. The natural ability of the slag phase to dissolve more efficiently (oxidic) precious metals species [25, 43] at increasing oxygen partial pressure is compensated and even superseded by changes in the thermodynamic properties of the matte, depleting the matte in iron and simultaneously increasing its sulfur deficiency. The trace elements studied in this paper also strongly favor the metal phase in copper–matte equilibria [48] which supports the observed behavior of matte–slag equilibria when the metallization degree of the matte increases as the matte composition approaches the blister copper saturation.

The very low PGE concentrations of silicate melts reported in some recent papers [49–51] are obviously due to too slow quenching and the precipitates not included in the LA-ICP-MS analyses. The lowest oxygen pressure of this study at 1250 °C was as low as $Log_{10}P_{O2} = -8.4$. It is not far from the experimental conditions of Ertel et al. and Amossé et al. [49–51], when extrapolated to 1200 °C, where the experimental point $Log_{10}P_{O2} = -9.0$ was used.

This paper gives new and accurate data on precious and platinum group metal distributions in copper smelting and the results can be used in more accurate estimations of their recoveries in the primary and secondary raw material processing [52, 53]. The results indicate that the matte–slag distribution equilibria are dominated by properties of the sulfide matte, in spite of the obvious dissolution of the trace elements in the slag predominantly as oxide species [44].

Conclusions

The distributions of precious metals (Ag, Au, Pd, Pt and Rh) between copper matte and slag in flash smelting are poorly known. This work gives new valuable experimental data about the distributions of the precious metals between copper matte and silica-saturated iron silicate slag at three

temperatures (1250, 1300, and 1350 °C) and under controlled CO–CO₂–SO₂–Ar gas atmospheres. An advanced experimental method (equilibration–quenching–EPMA/LA-ICP-MS) was applied in this study, which improved the accuracy and reliability of the solubility observations. This is the first report of the LA-ICP-MS analysis method being adopted to detect minor elements in metallurgical iron silicate slags.

Silver solubility in slag varied between 40 and 80 ppm and the distribution coefficient between 100 and 200 in the matte grade range of 50–70 % Cu. These results agree well with the previous results [8, 13]. For other precious metals, the solubilities in iron silicate slags were only between 1 and 20 ppm and the trend was decreasing with matte grade. The distribution coefficients in a matte grade of 65 % Cu were gold 1500, palladium 3000, platinum 6000, and rhodium 10,000. The distribution mechanism of the trace elements between iron silicate slag and copper matte appear to be dominated by properties of the matte phase.

References

1. Nansai K, Nakajima K, Kagakawa S, Kondo Y, Shigetomi Y, Suh S (2015) Global mining risk footprint of critical metals necessary for low-carbon technologies: the case of neodymium, cobalt, and platinum in Japan. Environ Sci Technol 49(4):2022–2031

2. Daurat M, Bringezu S (2009) Platinum Group Metal Flows of Europe, Part II. Exploring the technological and institutional potential for reducing environmental impacts. J Environ Ecol 13(3):406–421

3. Critical raw materials for the EU. Report of the Ad hoc Working Group on defining critical materials. Version of 30 July, 2010. http://ec.europa.eu/enterprise/policies/rawmaterials/documents/index_en.htm

4. Daurat M, Bringezu S (2008) Platinum Group Metal Flows of Europe, Part I. Global supply, use in industry, and shifting of environmental impacts. J Environ Ecol 12(5/6):754–767

5. Cabri LJ (1992) The distribution of trace precious metals in minerals and mineral products. Mineral Mag 56(384):289–308

6. Graedel TE, Bertram M, Fuse K, Gordon RB, Lifset R, Rechberger H, Spatari S (2002) The contemporary European copper cycle: the characterization of technological copper cycles. Ecol Econ 42(1–2):9–26

7. Reuter M, Kojo IV (2014) Copper: a key enable of resource efficiency. World Metall-Erzmetall 67(1):5–12

8. Roghani G, Takeda Y, Itagaki K (2000) Phase equilibrium and minor element distribution between FeOₓ-SiO₂-MgO-based slag and Cu₂S-FeS matte at 1573 K under high partial pressures of SO₂. Metall Mater Trans B 31B(4):705–712

9. Takeda Y, Roghani G (1993) Distribution equilibrium of silver in copper smelting system. In: Henein H, Oki T (eds) Proceedings of

First International Conference on Processing Materials for Properties. TMS, Warrendale (PA) USA, pp 357–360

10. Roghani G, Hino M, Itagaki K (1997) Phase equilibrium and minor element distribution between slag and copper matte under high partial pressures of SO_2. In: Proceedings of 5th International Conference on Molten Slags, Fluxes and Salts. Iron Steel Soc, Warrendale, pp 693–703

11. Louey R, Swinbourne D, Lehner T (1999) Silver and tin distribution between copper matte and fayalite slag. Aus IMM Proc 304(2):31–36

12. Kashima M, Eguchi M, Yazawa A (1978) Distribution of impurities between crude Cu, white metal and silica-saturated slag. Trans Jpn Inst Met 19(3):152–158

13. Avarmaa K, Johto H, Taskinen P (2014) Distribution of precious metals (Ag, Au, Pd, Pt, and Rh) between copper matte and iron silicate slag. Metall Mater Trans B (submitted)

14. Henao HM, Yamaguchi K, Ueda S (2006) Distribution of precious metals (Au, Pt, Pd, Rh and Ru) between copper matte and iron-silicate slag at 1573 K. In: Kongoli F, Reddy R (eds) Proceedings of Sohn International Symposium, vol. 1. TMS, Warrendale, pp 723–729

15. Hidayat T, Hayes PC, Jak E (2012) Experimental study of ferrous calcium silicate slags: phase equilibria at P_{O_2} between 10^{-8} atm and 10^{-9} atm. Metall Mater Trans B 43B(1):27–38

16. Xu X, Hayes P, Jak E (2012) Phase equilibria in the "SnO"-SiO_2-"FeO" system in equilibrium with tin-iron alloy and the potential application for electronic scrap recycling. Int J Mater Res 103(5):529–536

17. Yazawa A (1974) Thermodynamic considerations of copper smelting. Can Metall Q 13(3):443–453

18. Davies RH, Dinsdale AT, Gisby JA, Robinson JAJ, Martin SM (2002) MTDATA-thermodynamic and phase equilibrium software from the National Physical Laboratory. Calphad 26(2):229–271

19. SGTE Database for Pure Substances, Scientific Group Thermodata Europe. http://www.sgte.org/

20. Pouchou JL, Pichoir F (1986) Basic expression of "PAP" computation for quantitative EPMA. In: Brown JD, Packwood RH (eds) 11th International congress on X-ray optics and microanalysis (ICXOM). Canada, Wiley, pp 249–253

21. Kato T (2005) New accurate bence-albee α-factors for oxides and silicates calculated from the pap correction procedure. Geostand Geoanal Res 29(1):83–94

22. Norman MD, Garcia MO, Bennett VC (2004) Rhenium and chalcophile elements in basaltic glasses from Ko'olau and Moloka'i volcanoes: magmatic outgassing and composition of the Hawaiian plume. Geochim Cosmochim Acta 68(18):3761–3777

23. Jochum KP, Weis U, Stoll B, Kuzmin D, Yang Q, Raczek I, Jacob DE, Stracke A, Birbaum K, Frick DA, Günther D, Enzweiler J (2011) Determination of reference values for NIST SRM 610–617 glasses following ISO guidelines. Geostand Geoanal Res 35:397–429

24. Paton C, Hellstrom JC, Woodhead JD, Hergt JM (2001) Iolite: freeware for the visualisation and processing of mass spectrometer data. JAAS 26:2508–2518

25. Mungall JE, Brenan JM (2014) Partitioning of platinum-group elements and Au between sulfide liquid and basalt and the origins of mantle-crust fractionation of the chalcophile elements. Geochim Cosmochim Acta 125(1):265–289

26. Borisov A, Palme H (1997) Experimental determination of the solubility of platinum in silicate melts. Geochim Cosmochim Acta 61(20):4349–4357

27. Lynch DC, Akagi S, Davenport WG (1991) Thermochemical nature of minor elements in copper smelting mattes. Metall Trans B 22B(5):677–688

28. Zhong T, Lynch DC (1998) Henrian activity coefficient of Pb in Cu-Fe mattes and white metal. Metall Mater Trans B 29B(2):429–436

29. Roine A, Jalkanen H (1985) Activities of As, Sb, Bi, and Pb in copper mattes. Metall Trans B 16B(2):129–141

30. Roine A (1987) Activities of As, Sb, Bi, and Pb in copper mattes—effect of O, Ni, and Co. Metall Trans B 18B(March):203–212

31. Roghani G, Hino M, Itagaki K (1997) Phase equilibrium and minor elements distribution between SiO_2-CaO-FeO_x-MgO slag and copper matte at 1573 K under high partial pressures of SO_2. Mater Trans JIM 38(8):707–713

32. Richardson F, Billington J (1956) Copper and silver in silicate slags. Trans Inst Min Metal 593:273–297

33. Nagamori M, Mackey PJ (1978) Thermodynamics of copper matte converting: part II. Distribution of Au, Ag, Pb, Zn, Ni, Se, Te, Bi, Sb and As between copper, matte and slag in the noranda process. Metall Trans B 9B(6):567–579

34. Roghani G, Font JC, Hino M, Itagaki K (1996) Distribution of minor elements between calcium ferrite slag and copper matte at 1523 K under high partial pressure of SO_2. Mater Trans JIM 37(10):1574–1579

35. Takeda Y (1983) Distribution equilibria of minor elements between liquid copper and calcium ferrite slag. Trans Jpn Inst Met 24(7):518–528

36. Subramanian PR, Chakrabarti DJ, Laughlin DE (eds) (1994) Phase diagrams of binary copper alloys, monograph series on alloy phase diagrams #10. ASM, Metals Park

37. Zakeri A, Hino M, Itagaki K (1989) Activity of silver in molten copper sulfide saturated with copper. Mater Trans JIM 39(11):1101–1107

38. Celmer RS, Toguri JM (1986) Cobalt and gold distribution in nickel-copper matte smelting. In: Ozberg E, Marcuson SW (eds) Nickel metallurgy, vol I. extraction and refining of nickel. Montreal, pp 147–163

39. Choi N, Cho W (1995) Distribution of cobalt, gold, and silver between matte and slag in nickel sulfide smelting. In: Reddy RG, Mishra B (eds) Trace and reactive metals: processing and technology. TMS, Warrendale, pp 55–63

40. Choi N, Cho WD (1998) Distribution of gold and silver between nickel-copper matte and silica-saturated iron silicate slag. Miner Metall Proc 15(3):23–29

41. Yamaguchi K (2010) Distribution of precious metals between matte and slag and precious metal solubility in slag. In: Proceedings of Copper 2010, vol 3. GDMB, Clausthal-Zellerfeld, Germany, pp 1287–1295

42. Borisov A, Palme H (1996) Experimental determination of the solubility of au in silicate melts. Min Petrol 56(3–4):297–312

43. Borisov A, Palme H, Spettel B (1994) Solubility of palladium in silicate melts: implications for core formation in the earth. Geochim Cosmochim Acta 58(2):705–716

44. Borisov A, Palme H (2000) Solubilities of noble metals in Fe-containing silicate melts as derived from experiments in Fe-free systems. Am Min 85:1673–2665

45. Yamaguchi K (2011) Distribution of platinum and palladium in iron oxide slags equilibrated with molten copper at 1573 K. In: Proceedings of European Metallurgical Conference EMC 2011, vol. 1. GDMB, Clausthal-Zellerfeld, Germany, pp 171–179

46. Abe T, Sundman B, Onodera H (2006) Thermodynamic assessment of the Cu-Pt system. J Phase Equil Diffus 27(1):5–13

47. Li M, Du Z, Guo C, Li C (2008) A thermodynamic modeling of the Cu-Pd system. Calphad 32(2):439–446

48. Taylor JR (1983) A thermodynamic study of the distribution of metals between copper matte and bullion. In: Sohn HY, George DB, Zunkel AD (eds) Advances in Sulfide Smelting, vol 1. TMS, Warrendale, pp 217–229

49. Ertel W, O'Neill HSC, Sylvester P (1999) Solubilities of Pt and Rh in a haplobasaltic silicate melt at 1300 °C. Geochim Cosmochim Acta 63(16):2439–2449

50. Amossé J (2000) Thermochemical behaviour of Pt, Ir, Rh and Ru vs f_{O2} and f_{S2} in a basaltic Melt. Implications for the differentiation and precipitation of these elements. Mineral Petrol 68(1):29–61

51. Dable P, Allibert M, Poignet JC, Amossé J (2001) Solubility of platinum and rhodium in lime-alumina-silica melts at 1700 K. J Am Ceram Soc 84(5):1097–1107

52. Nakajima K (2011) Thermodynamic analysis for the controllability of elements in the recycling process of metals. Environ Sci Technol 45(11):4929–4936

53. Stamp A, Althaus H-J, Wäger PA (2013) Limitations of applying life cycle assessment to co-product systems: the case of an integrated precious metals smelter-refinery. Res Conserv Recycl 80(1):85–96